

Journal of Materials Chemistry B

Accepted Manuscript



This article can be cited before page numbers have been issued, to do this please use: X. Dong, H. Shi, W. Sun, C. Liu, G. Gu, B. Ma, W. Si, N. Fu, Q. Zhang and W. Huang, *J. Mater. Chem. B*, 2015, DOI: 10.1039/C5TB02041G.



This is an *Accepted Manuscript*, which has been through the Royal Society of Chemistry peer review process and has been accepted for publication.

Accepted Manuscripts are published online shortly after acceptance, before technical editing, formatting and proof reading. Using this free service, authors can make their results available to the community, in citable form, before we publish the edited article. We will replace this *Accepted Manuscript* with the edited and formatted *Advance Article* as soon as it is available.

You can find more information about *Accepted Manuscripts* in the [Information for Authors](#).

Please note that technical editing may introduce minor changes to the text and/or graphics, which may alter content. The journal's standard [Terms & Conditions](#) and the [Ethical guidelines](#) still apply. In no event shall the Royal Society of Chemistry be held responsible for any errors or omissions in this *Accepted Manuscript* or any consequences arising from the use of any information it contains.

Tumor-Targeting and Enzyme-Activated Nanoparticles for Simultaneous Cancer Diagnose and Photodynamic Therapy

Huaxia Shi,^a Wucheng Sun,^a Changbing Liu,^a Guiying Gu,^c Bo Ma,^c Weili Si,^b Nina Fu,^a

Qi Zhang,^{*c} Wei Huang,^{*ab} and Xiaochen Dong^{*b}

^aKey Laboratory for Organic Electronics & Information Displays (KLOEID), Nanjing University of Posts and Telecommunications, Nanjing 210023, China.

^bKey Laboratory of Flexible Electronics (KLOFE) & Institute of Advanced Materials (IAM), Jiangsu National Synergetic Innovation Center for Advanced Materials (SICAM), NanjingTech University (NanjingTech), 30 South Puzhu Road, Nanjing 211816, China.

E-mail: iamxcdong@njtech.edu.cn, iamwhuang@njtech.edu.cn

^cSchool of Pharmaceutical Science, Nanjing Tech University (NanjingTech), 30 South Puzhu Road, Nanjing 211816, China. Email: zhangqi@njtech.edu.cn

Specific targeting towards tumors and on-site activation of photosensitizers to diagnose tumors and reduce side effects for patients are main challenges for current photodynamic therapy (PDT), in clinic. Herein, uniform diiodostyryl bodipy conjugated hyaluronic acid nanoparticles (DBHA-NPs) were successfully synthesized. PDT effect evaluated in both cell level and animal models of tumor-bearing mice shows that the DBHA-NPs present a remarkable suppression of tumorous growth due to their specific targeting and enhanced permeability and retention (EPR) effect. More importantly, enzyme-activated “self-assembly and disaggregation” behavior made by tumors can lead DBHA-NPs on-site activation, which can diagnose the tumor exactly and reduce side effect for patients significantly. These findings confirm that DBHA-NPs have a significant potential for photodynamically activated cancer theranostics, in clinic.

1. Introduction

Photodynamic therapy (PDT) is an effective therapeutic modality for a variety of malignant and nonmalignant tumors.¹⁻⁴ Mediated by photosensitizers (PSs), cancer cells can be killed by reactive oxygen species (ROS), which are generated from locally sensitizing oxygen upon light irradiation.⁵ As for cancer treatment, PDT has emerged as an important method in preclinical research and clinical practice because of its non-invasive property and selective light irradiation on tumor site, avoiding normal tissues and organs being damaged.

However, there are still several problems to prevent the development of PDT in clinic. First, traditional PSs suffer from their native hydrophobicity and poor biocompatibility, limiting their potential application in biological field.⁶ At present, two main strategies have been developed to increase their water solubility and biocompatibility. On the one hand, PSs can be conjugated with hydrophilic molecule through covalent bond.⁷ On the other hand, PSs can be incorporated into biocompatible drug delivery platforms via noncovalent bond, such as liposomes,⁸⁻¹¹ polymeric micelles,¹²⁻¹⁴ and inorganic nanoparticles.¹⁵⁻²⁰ Second, how to enhance the selectivity of highly effective PSs so that they can locate and function at tumor site preferentially is another major challenge. A promising method is to directly conjugate PSs with targeting ligands, including folates, antibodies, proteins, and so on.²¹⁻²³ And, the third obstacle for PDT in clinic is that activation of PSs at non-tumor site would damage normal tissues and organs of patients through blood circulation. Recently, activatable photosensitizing systems have drawn a lot of attention, which can be

activated selectively by tumors-associated stimuli. Commonly, activatable PSs are photodynamic inactive in normal tissue environment and their fluorescence and ROS generation are silent even with light irradiation. However, these PSs become photodynamically active in tumor site through various kinds of activation mechanisms, including enzymatic activation,^{24, 25} nucleic acid-activation^{26,27} and tumor environmental activation²⁸ (e.g., remarkable decrease in pH value and significant increased level of H₂O₂). The activatable PSs can achieve excellent treatment selectivity and destroy targeted tumor cells, but not threat normal tissues and organs²⁹. Therefore, the development of new kinds of PSs to solve all these problems mentioned above in PDT clinic is extremely important.

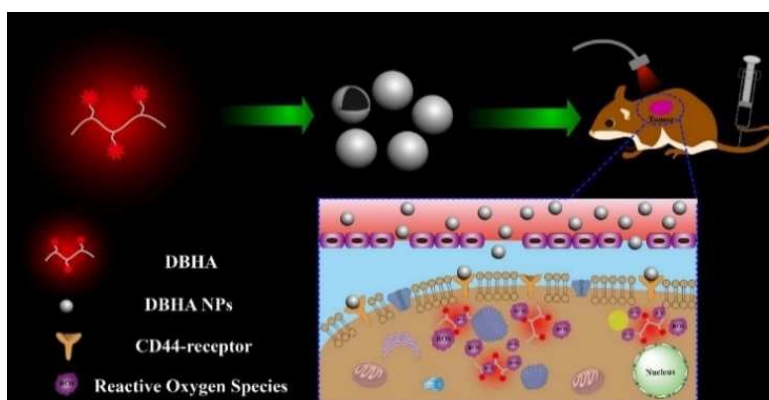


Fig. 1 Schematic illustration of DBHA-NPs as theranostic agents for PDT both in vitro and in vivo.

In this study, diiodostyryl bodipy conjugated hyaluronic acid nanoparticles (DBHA-NPs) are designed for activatable photodynamic theranostics in tumors. The DBHA-NPs exhibit excellent hydrophilicity and biocompatibility, as well as specific targeting towards CD44 receptor overexpressed on the surface of tumor cells (e.g. HCT-116 cells, human colon carcinoma cell line). And the DBHA-NPs reaching into

the lysosomes inside HCT-116 cells can be disaggregated, resulting in the restoration of fluorescence and ROS with light irradiation, which is impossible in the native of diiodostyryl bodipy due to its aggregation (Fig. 1). Additionally, both in vitro and in vivo experiments demonstrate that DBHA-NPs can effectively label and photodynamically suppress the growth of tumor.

2. Experimental Section

Synthesis of DBHA-NPs

Fig. 2 shows the synthetic route of DBHA. In brief, 4-hydroxybenzaldehyde was treated with 3-bromo-1-propanol in the presence of K_2CO_3 in acetone to yield Compound 1. And diiodo bodipy^{30, 31} (Compound 3) was prepared through iodination of bodipy^{32, 33} (Compound 2), using N-iodosuccinimide (NIS) as iodo-agent. Furthermore, Compound 3 underwent Knoevenagel condensation with Compound 1 to yield diiodostyryl bodipy (Compound 4) through microwave reaction.³⁴ As well known, diiodostyryl bodipy has great potential as PS for PDT, mainly suffering from its native hydrophobicity and bad biocompatibility, as well as targeting.³⁵⁻³⁷ It can be concluded that the above diiodostyryl bodipy (Compound 4) is further conjugated onto the hyaluronic acid (HA) through esterification reaction. Notably, DBHA shows excellent water-solubility and good biocompatibility due to the existence of HA. And finally, DBHA dissolved into deionized (DI) water was dropwise added into large amount of DI water under the ultrasound to yield DBHA-NPs through self-assembly.

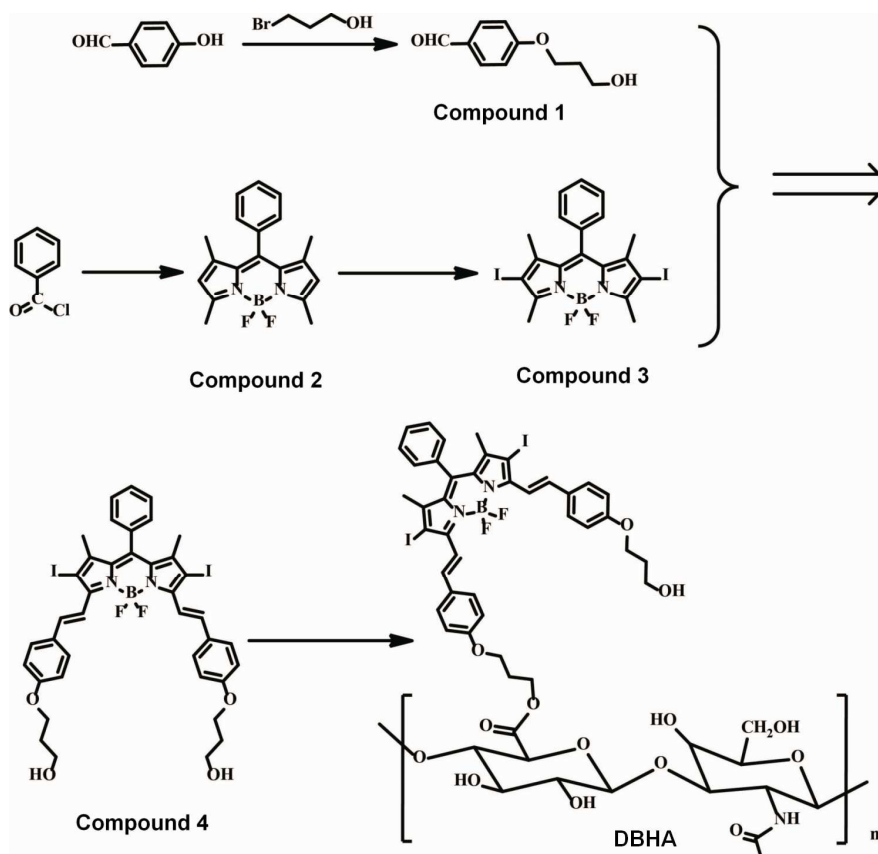


Fig. 2 Synthetic route of DBHA.

Characterization

Nuclear magnetic resonance (NMR) spectra were measured by using a Bruker Ultra Shield Plus 400 MHz. GC-MS was recorded on a Shimadzu GC-MS-QP 2010 Plus mass spectrometer. MALDI-TOF-MASS (Matrix-assisted laser desorption/ionization time-of-flight mass spectrometry) was performed on a Bruker autoflex under the reflector mode (without the matrix) for data acquisition. The UV-visible absorption and photoluminescence (PL) spectra were recorded on a Shimadzu UV-3600 UV-VIS-NIR spectrophotometer and a RF-5301 PC spectrofluorophotometer, respectively. Transmission electron microscopy (TEM) images were obtained using a JEOL JEM-2100 transmission electron microscope. The hydrodynamic size of the

nanoparticles (Dynamic light scattering, DLS) was measured by using a 90 Plus particle size analyzer, Brookhaven Instruments.

Cell Lines and Culture Conditions

HCT-116 and A2780 cell lines, provided by the Institute of Biochemistry and Cell Biology, SIBS, CAS (China), were cultured in regular growth medium consisting of Dulbecco's modified Eagle's medium (DMEM, Gibco) supplemented with 10% fetal bovine serum at 37 °C under 5% CO₂ atmosphere. The cells were routinely harvested by treating with a trypsin-ethylene diamine tetraacetic acid (EDTA) solution (0.25%).

Cell Viability Assays

HA and DBHA-NPs were first dissolved in phosphate buffered saline (PBS) solution, then diluted with DMEM to various concentrations (0.2, 0.4, 0.6, 0.8, 1.0, 1.2, 1.4, and 1.6 mg/ml). HCT-116 cells and A2780 cells, rinsed with PBS solution, were incubated with HA and DBHA-NPs solutions for 24 h at 37°C. Then the cells were rinsed again with PBS solution and refilled with 100 μL of the culture medium before being illuminated at ambient temperature. The light source was from Xenon lamp, equipped with a color glass filter with cut-on at 600 nm. The fluence rate ($\lambda > 600$ nm) was 40 mW/cm² for 7 minutes.

Cell viability was determined by means of the colorimetric MTT assay. An MTT (USB) solution in PBS solution (5 mg/mL, 20 μL) was added into each well followed by incubation for 4 h under the same environment at 37 °C. Then the medium was discarded and 150 μl DMSO was added. The plate was agitated on a Bio-Tek microplate reader at ambient temperature before the absorbance at 490 nm for each

well was taken. The average absorbance of the blank well, no cells, was subtracted from the readings of the other wells. The cell viability was then determined by the following equation: Viability (%) = $\{\sum [(A_i/A_{control}) * 100]\} / n$, where A_i is the absorbance of i th data ($i = 1, 2, 3 \dots, n$), $A_{control}$ is average absorbance of the control wells in which HA or DBHA-NPs was absent, and n is the number of the data points.

Flow Cytometric Study

Approximately 6×10^5 HCT-116 cells in the medium (2 mL) were seeded on a 6-well plate and incubated for 24 h under 5% CO₂. The cells were treated with DBHA-NPs at various concentrations (0.25, 0.5, 0.75, and 1.0 mg/ml) and incubated under the same conditions for 4 h. The cells were then rinsed thrice with PBS solution and refilled with 1 ml of the culture medium before being illuminated ($\lambda > 600$ nm, 40 mW/cm², 7 min) at ambient temperature. After 24 h of incubation, the cell were rinsed with PBS solution and harvested by 0.25% trypsin (Invitrogen, 500 μ L) for 2 min, followed by centrifugation at 1200 rpm. The cells were suspended in 100 μ l of binding buffer containing FITC annexin-V (5 μ l) and PI (5 μ l). After incubation in darkness for 15 min at room temperature, the signals of FITC annexin-V and PI were measured by a BD FACSCalibur flow cytometer (Becton Dickinson) with 10^4 cells counted in each example. Both annexin-V and PI were excited by a 488 nm argon laser. The emitted fluorescence was monitored at 500-560 nm for annexin-V and at > 670 nm for PI. The data collected were analyzed by using Cell QUEST Pro.

Fluorescence Microscopic Study

About 2×10^5 HCT-116 cells or A2780 cells in the culture medium (2 ml) were seeded

on a glass bottom Petri dish and incubated overnight at 37 °C. Then the medium was removed. The cells, rinsed with PBS solution, were incubated with solution of DBHA-NPs (1 mg/ml, 100 µl) in the medium for 4 h. The cells were rinsed with PBS solution and viewed with an Olympus IX 70 inverted microscope. The excitation light (588 nm) was provided by a multi-wavelength illuminator (Polychrome IV, TILL Photonics). The emitted fluorescence at > 600 nm was collected, digitized, and analyzed using MetaFluor V 6.3 (Universal imaging). The average intracellular fluorescence intensities (24 cells for each sample) were determined.

To confirm the concept of CD44-receptor mediated tumor cell endocytosis, similarly, about 2×10^5 HCT-116 cells in the culture medium (2 ml) were seeded on a glass bottom Petri dish and incubated overnight at 37 °C under 5% CO₂. Then the medium was removed. Firstly, the cells were incubated with HA solution (2 mg/ml, 100 µl) for 4 h, further rinsed with PBS solution. Then the above cells were incubated with DBHA-NPs solution (1 mg/ml, 100 µl) for 4 h under the same concentrations. The cells were rinsed with PBS solution and viewed with an Olympus IX 70 inverted microscope. The excitation light (588 nm) was provided by a multi-wavelength illuminator (Polychrome IV, TILL Photonics). The emitted fluorescence at > 600 nm was collected, digitized, and analyzed using MetaFluor V 6.3 (Universal imaging).

Subcellular Location Study

About 1×10^5 HCT-116 cells in culture medium (2 ml) were seeded on glass bottom Petri dish and incubated overnight at 37 °C under 5% CO₂. The medium was removed and the cells were rinsed with PBS solution. The cells were incubated with

DBHA-NPs solution in the medium (1 mg/ml, 100 μ l) for 24 h. For the study using Mito-Tracker, the cells were incubated with Mito-Tracker Green FM (Molecular Probes, 0.2 μ M in the medium) for further 15 min. For the study using Lyso-Tracker, green DND 26 (Molecular Probes, 0.075 μ M in the medium) or ER-Tracker Green (Molecular Probes, 1.0 μ M in PBS solution) for further 15 min. For all the cases, the cells were rinsed with PBS solution and viewed with a Leica SP5 confocal microscope equipped with a 488 nm argon laser and a 588 nm helium neon laser. All trackers were excited at 488 nm and monitored at 510-560 nm, while DBHA-NPs were excited at 588 nm and monitored at 600-700 nm. The images were digitized and analyzed using the Leica Application Suite Advanced Fluorescence software. The subcellular location of DBHA-NPs was revealed by comparing the intracellular fluorescence images caused by the Mito-Tracker, Lyso-Tracker, ER-Tracker and DBHA-NPs.

Real-time monitoring the fluorescence in vitro

About 1×10^5 HCT-116 cells in culture medium (2 ml) were seeded on glass bottom Petri dish and incubated overnight at 37 $^{\circ}$ C under 5% CO₂. The medium was removed, and the cells were rinsed with PBS solution, followed adding a solution of DBHA-NPs (1 mg/ml, 100 μ l) into fresh medium for incubation at 37 $^{\circ}$ C. Meantime, the fluorescence of DBHA-NPs was observed by Confocal Laser Scanning Microscope (CLSM) and the confocal images were obtained by using Zeiss confocal laser microscope (ZEISS LSM 700) at different time.

Fluorescence Studies for ROS probe

About 2×10^5 HCT-116 cells in the culture medium (2 ml) were seeded on glass bottom Petri dish and incubated overnight at 37 °C under 5% CO₂. The medium was removed. The cells, rinsed with PBS solution, were incubated with a solution of DBHA-NPs or Porphyrin in PBS solution (1 mg/ml, 100 µl) for 24 h. The cells were rinsed with PBS solution and further incubated with ROS probe, DCFH-DA (50 µg/ml, 10 µl) for 1 h. And then, the cells were rinsed thrice with PBS solution and refilled with 1 ml of the culture medium before being illuminated at ambient temperature using a Xenon lamp light ($\lambda > 600$ nm, 40 mW/cm², 7 min). After that, the cells were viewed with Olympus IX70 inverted microscope. The excitation light (488 nm) was provided by a multi-wavelength illuminator (PolychromeIV, TILL Photonics). The emitted fluorescence from 500 to 600 nm was collected, digitized, and analyzed using MetaFluor V 6.3 (Universal imaging).

For comparison without cells, no cells were added and only DBHA-NPs or Porphyrin with DCFH-DA at the same concentrations.

In vivo fluorescence and Cancer treatment

All animal experiments were performed complying with the NIH guidelines for the care and use of laboratory animals. The xenograft tumors were established subcutaneously injecting HCT-116 cells into the armpit of nude mice. After tumors of 30-40 mm³ were palpable, whole body images of mice were acquired respectively by a tail vein injection of 200 µl of DBHA-NPs at a concentration of 10 mg/ml. All images were analyzed and collected at the indicated time points with a MaestroTM In-Vivo Imaging System (Cri, Woburn, MA, USA).

For the tumor treatment, the mice were divided into four groups with six mice in each group, randomly. The mice in the first to the third group were injected with saline, HA and DBHA-NPs solution (10 mg/ml, 200 μ l) by a tail vein injection, respectively, with light irradiation ($\lambda > 600$ nm, 40 mW/cm², 15 min). And the mice in the fourth group were injected with DBHA-NPs solution (10 mg/ml, 200 μ l) by a tail vein injection without light irradiation while under the same conditions.

3. Results and discussion

Preparation and characterization of DBHA-NPs

Fig. 3a shows the ¹H-NMR spectrum of DBHA in D₂O. The appearance of chemical shifts between 7.0-8.0 in the spectra compared with that of HA^{38,39} suggests that HA has successfully conjugated onto the diiodostyryl bodipy. The TEM image in Fig. 3b demonstrates that the self-assembled DBHA-NPs have spherical morphology. The dynamic light scattering (DLS) measurement indicates the average size of the particles is around 50 nm (Inset in Fig. 3b). Fig. 3c shows the optical absorption properties of DBHA, DBHA-NPs and HA dissolved in PBS, respectively. An obvious absorption peak at 600 nm arising from the Q-band of diiodostyryl bodipy can be observed. On the contrary, there are no peaks for pure HA, indicating that diiodostyryl bodipy has been successfully conjugated onto the HA. Interestingly, after the addition of hyaluronidase which can degrade HA polymer, the fluorescence of diiodostyryl bodipy (at 678 nm) recovers in a time-dependent manner (Fig. 3d and S1), confirming the enzymatic degradation process of HA. With the degradation of HA, DBHA NPs can also be de-aggregated and the fluorescence intensity increases.

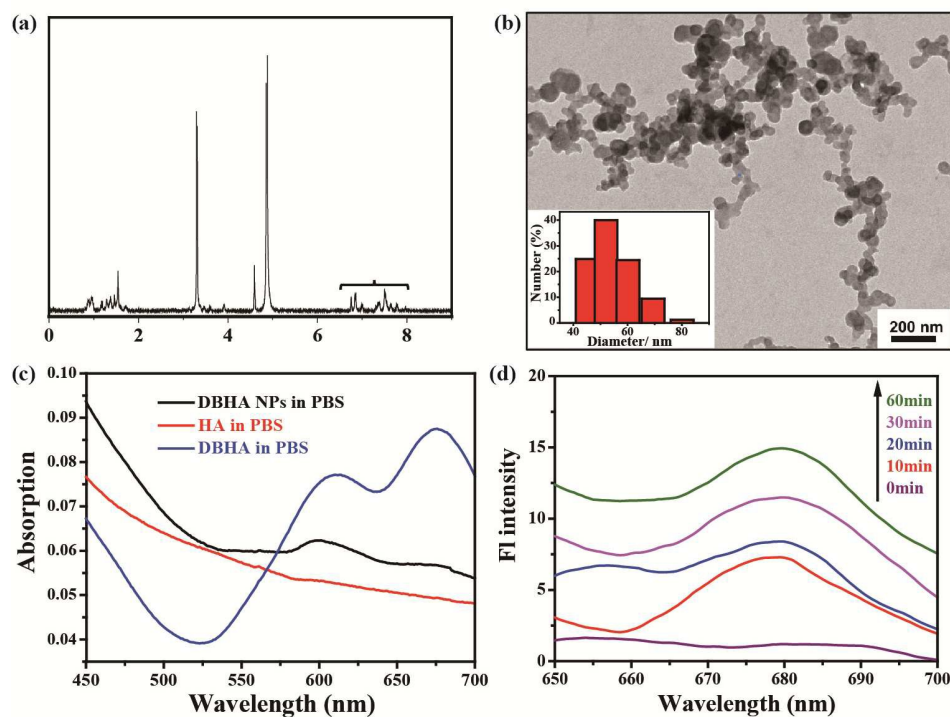


Fig. 3 (a) $^1\text{H-NMR}$ spectrum of DBHA in D_2O . (b) TEM image of DBHA-NPs. The inset shows the size distribution of DBHA-NPs. (c) UV-Vis absorption of DBHA, DBHA-NPs and HA (5 mg/ml) in PBS. (d) Fluorescence spectra of DBHA-NPs (5 mg/ml) incubated with hyaluronidase (0.1 mg/ml) in PBS for different time, excited at 600 nm.

NIR fluorescence images and specific targeting of DBHA-NPs

CD44, a receptor for HA, is overexpressed in some types of cancer cells (e.g., HCT-116 cells, corresponding to colon cancer).⁴⁰ As expected in Fig. 4a, the DBHA-NPs can abundantly stain the HCT-116 cells⁴¹ and uniformly dispersed in the cytoplasm of HCT-116 cells. On the contrary, A2780 cells (human ovarian carcinoma cell line), known to have low expression of CD44 receptors, are not well-stained by DBHA-NPs and the fluorescence intensity is greatly decreased compared with that of HCT-116 cells (Fig. 4b). It is well known that the staining can be eliminated by the

previous addition of excess free HA molecules because of the competitive inhibition. As shown in Fig. 4b, with the existence of HA, the fluorescence intensity of the HCT-116 cells decreases greatly, further indicating DBHA-NPs have specific targeting properties towards CD44 overexpressed HCT-116 cells. And all the results suggest that DBHA-NPs are internalized via receptor mediated endocytosis triggered by the binding of DBHA-NPs with CD44 receptor.⁴² What's more, the parallel filter evaluation indicates that the DBHA-NPs are mainly delivered into lysosomes, as shown in Fig. 4c and Fig. S2.

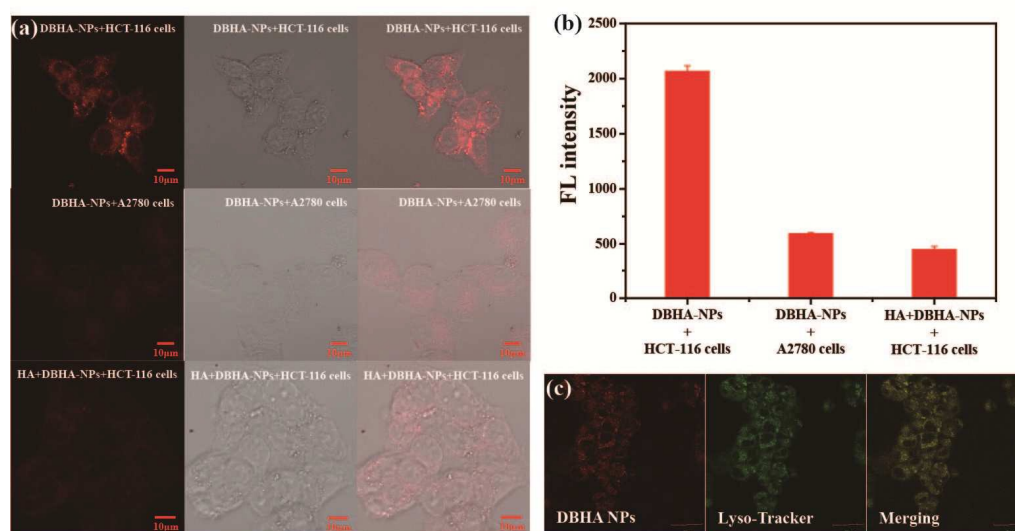


Fig. 4 (a) Fluorescence images of DBHA-NPs in HCT-116 cells, A2780 cells and HA+DBHA-NPs in HCT-116 cells, respectively. Red color represents the fluorescence of DBHA-NPs. (Left panel, fluorescence images. Middle panel, bright field. Right, merged images). (b) The intracellular fluorescence intensity of DBHA-NPs in HCT-116 cells, in A2780 cells and HA+DBHA-NPs in HCT-116 cells. All data were expressed as the mean \pm standard deviation (number of experiments, $n=6$). (c) Visualization of the intracellular fluorescence of HCT-116 cells using filter

sets specific for DBHA-NPs (in red, column 1) and lysosome tracker (in green column 2). Column 3 is the merged images in bright field.

NIR fluorescent enzyme-activated of DBHA-NPs on tumorous site both in vitro and in vivo

To investigate the on-site activation properties of the DBHA-NPs in tumors, in vitro and in vivo fluorescence images of DBHA-NPs entering into HCT-116 cells at different time are measured. Fig. 5a presents the fluorescence images of DBHA-NPs incubating with HCT-116 cells with time observed by confocal laser scanning microscopy (CLSM). It can be found that the fluorescence becomes stronger and stronger with time from 0 to 60 minutes. Similar phenomena has also been observed in vivo after injection of DBHA-NPs in mice bearing HCT-116 cells, as shown in Fig. 5b. There is no obvious fluorescence observed before 8h, even in heart, liver, lung, brain and other organs and tissues.⁴³⁻⁴⁵ And the strong fluorescence only appears in the tumor site after 24 h after administration of DBHA-NPs. Both results indicate that DBHA-NPs only can be decomposed in cells or tumors, which is an effective on-site activated PSs and beneficial for diagnosing the tumor site exactly. Furthermore, this result is also coincidence well with the previous characterization (Fig. 3d).

Enzyme-activated generation of ROS

Reactive oxygen species (ROS) generated from PSs can cause an oxidative stress and membrane damage in the treated cells and eventual cell death, which is an important factor for PDT. 2',7'-dichlorofluorescein diacetate (DCFH-DA), non-fluorescence in its native, can react with ROS to produce fluorescent 2',7'-dichlorofluorescein

(DCF),⁴⁶ which is selected as ROS probe to identify the produced ROS by DBHA-NPs upon light irradiation. As shown in Fig. 5c, after DCFH-DA incubated with DBAH-NPs, the fluorescence intensity of DCF becomes stronger and stronger along with time from 0 to 60 min under light irradiation, indicating the concentration of ROS increases greatly with the incubated time prolonging. More interestingly, no fluorescence of DCF can be detected before DBHA-NPs enter into HCT-116 cells. It is quite different from the commercial PSs (porphyrin), which shows strong fluorescence both out of and inside HCT-116 cells (Fig. 5d). This phenomenon further demonstrates that DBHA-NPs only can react in tumor cells and realize the on-site activation.

As is described above in Fig. 4c, DBHA-NPs mainly locate in the lysosomes after entering into HCT-116 cells. And lysosomes are full of enzymes, such as hyaluronidase, which can make HA degradation and increase the fluorescence intensity of DBHA-NPs (Fig. 3d). It can be speculated that HA, the backbone of DBHA, can be degraded by hyaluronidase after the DBHA-NPs reach into lysosomes and realize fluorescence and ROS on-site activation in tumor cells. In clinic, on-site activation of PSs can be used in cancer diagnose and also provide a significant strategy for no avoiding light to reduce the side effects during the progress of PDT.⁴⁷

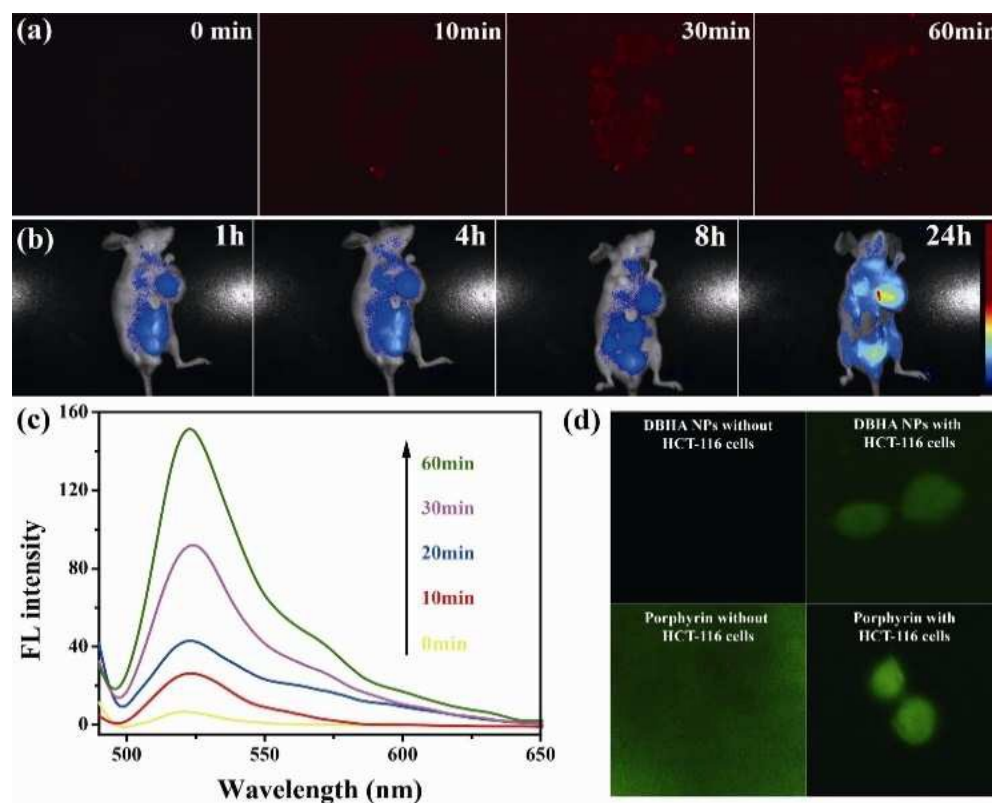


Fig. 5 (a) Fluorescence images of DBHA-NPs entering into HCT-116 cells observed by CLSM from 0 to 60 min. (b) In vivo fluorescence images of mice bearing HCT-116 cells in armpit after tail-vein injection of DBHA-NPs. (c) Fluorescence intensity of ROS probe after incubating with DBHA-NPs and hyaluronidase with light irradiation for different time. (d) Fluorescence images of DBHA-NPs and porphyrin with DCFH-DA out of or in HCT-116 cells upon light irradiation by CLSM. Column 1, DBHA NPs and porphyrin with DCFH-DA out of HCT-116 cells. Column 2, DBHA-NPs and porphyrin with DCFH-DA in HCT-116 cells.

Photodynamic efficiency of DBHA-NPs in vitro and in vivo

Encouraged by the above measurements, photodynamic activities of DBHA-NPs were further investigated against tumor cells. As shown in Fig. 6a, DBHA-NPs show higher phototoxicity and lower dark toxic, as well as dose-dependent survival curves, which

is in accord well with the flow cytometric assay of DBHA-NPs (Fig. S2). More importantly, the DBHA-NPs exhibit highly selective phototoxicity towards HCT-116 cells (CD44+receptor) compared with A2780 cells (CD44-receptor), indicating their high targeting property towards HCT-116 cells. In contrast, HA is non-toxic towards HCT-116 cells. It can be concluded that the photodynamic activities of DBHA-NPs originate from diiodo styryl bodipy, instead of HA. What's more, from the results of flow cytometric assay (Fig. S3), it can be speculated that the death mechanism of tumor cells is mainly late-apoptotic.

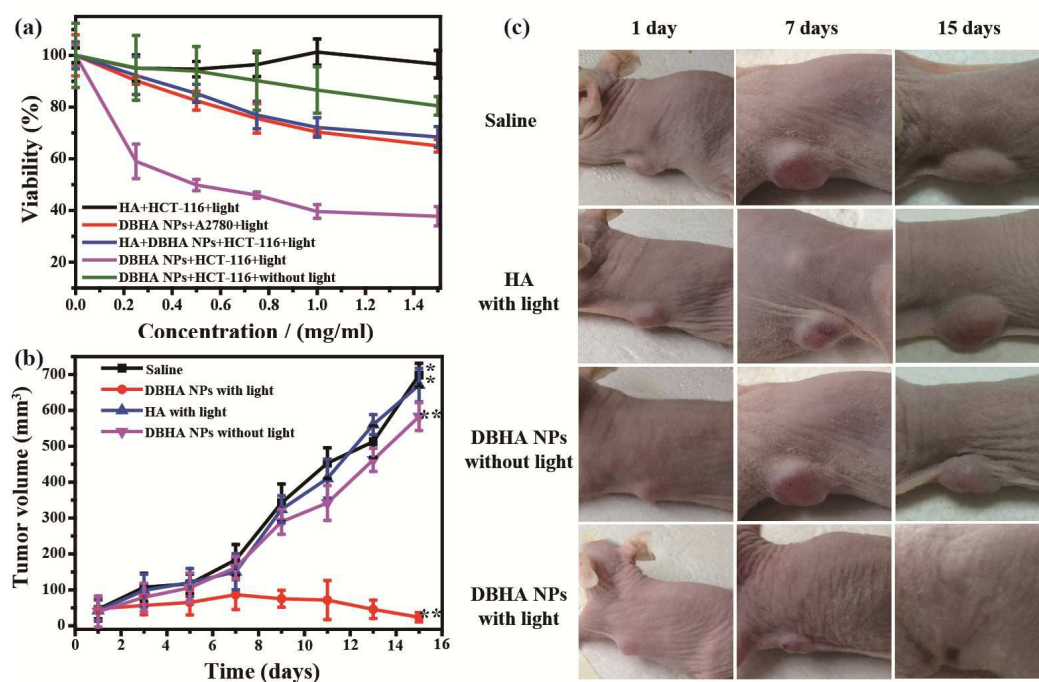


Fig. 6 (a) Comparison of cell viabilities by MTT assays ($\lambda > 600\text{nm}$). (b) The relationship between tumor volume and treated time of DBHA-NPs in the HCT-116 tumor cells bearing mouse model via tail vein injection. Twenty-four mice were randomly assigned into four groups (6 mice/groups), including saline with light, HA with light, DBHA-NPs without light and DBHA-NPs with light. (c) Typical

photographs of tumor-bearing mice treated at different time. Note, $*p < 0.05$, $**p < 0.01$.

To validate the practical application of DBHA-NPs, cancer treatments in vivo have been employed by using mice bearing HCT-116 cells. These mice are divided into four groups (6 mice each group), which were intravenously injected with saline, HA and DBHA-NPs with or without light irradiation, respectively, and followed by monitoring their tumor growth volume and body weight for fifteen days. Fig. 6b and 6c show the changes of tumor volume of mice during the treatment, respectively. The results indicate that the tumor volume of mice treated with saline and HA followed by light irradiation and DBHA-NPs without light irradiation experienced a rapid growth through the entire treatment period. However, the tumor growth of mice treated with DBHA NPs followed by light irradiation is obviously suppressed. It suggests that the DBHA-NPs can selectively accumulate in the malignant tumor, then inhibit the tumor growth upon light irradiation through the specific targeting, as well as the enhanced permeability and retention effect (“EPR” effect).⁴⁸⁻⁵⁰ Furthermore, no weight loss for therapeutic group was observed, just as same as the controlled group (Fig. S4), indicating that all the treatments were not severely toxic. It can be concluded that DBHA-NPs not only can serve as an efficient PS for cancer treatment, but also provide a significant strategy in clinic to solve the problem of non-tumor site activation of PSs, further reducing side effect for patients.

4. Conclusions

In summary, DBHA-NPs for cancer photodynamic theranostics have been

successfully synthesized. Originating from CD44 receptor overexpressed towards tumor cells by HA, as well as EPR effect, DBHA-NPs present specific targeting towards HCT-116 cells. What's more, on-site activation of DBHA-NPs by tumors can realize the tumor diagnose exactly and effectively overcome the problem of avoiding lighting to reduce side effects for patients significantly. In particular, both in vitro and in vivo experiments demonstrate that DBHA-NPs can effectively suppress tumor growth, which exhibits a great potential in photodynamically activatable cancer theranostics, in clinic.

Acknowledgements

The project was supported by 973 program (2014CB660808), Key University Science Research Project of Jiangsu Province (15KJA430006), Jiangsu Provincial Funds for Distinguished Young Scholars (BK20130046), the NNSF of China (61525402, 21275076, 61328401, 51103074), Program for New Century Excellent Talents in University (NCET-13-0853), Qing Lan Project, Synergetic Innovation Center for Organic Electronics and Information Displays, the Priority Academic Program Development of Jiangsu Higher Education Institutions (PAPD).

References

- 1 D. E. Dolmans, D. Fukumura and R. K. Jain, *Nat. Rev. Cancer.*, 2003, **3**, 380-387.
- 2 D. Bechet, S. R. Mordon, F. Guillemain and M. A. Barberi-Heyob, *Cancer. Treat. Rev.*, 2014, **40**, 229-241.
- 3 A. Kamkaew, S. H. Lim, H. B. Lee, L. V. Kiew, L. Y. Chung and K. Burgess, *Chem. Soc. Rev.*, 2013, **42**, 77-88.

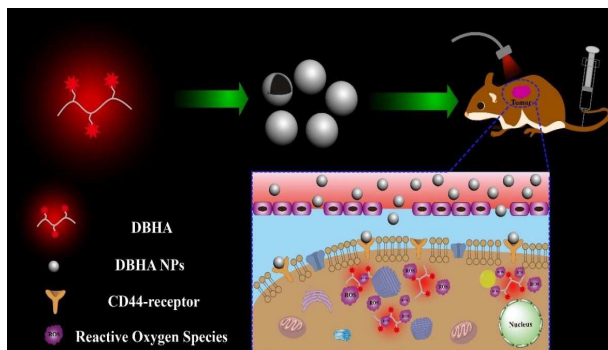
- 4 L. Cheng, C. Wang, L. Feng, K. Yang and Z. Liu, *Chem. Rev.*, 2014, **114**, 10869-10939.
- 5 H. Yuan, H. Chong, B. Wang, C. Zhu, L. Liu, Q. Yang, F. Lv and S. Wang, *J. Am. Chem. Soc.*, 2012, **134**, 13184-13187.
- 6 C. K. Lim, J. Shin, I. C. Kwon, S. Y. Jeong and S. Kim, *Bioconjugate Chem.*, 2012, **23**, 1022-1028.
- 7 D. S. Kwag, N. M. Oh, Y. T. Oh, K. T. Oh, Y. S. Youn and E. S. Lee, *Inter. J. Pharm.*, 2012, **431**, 204-209.
- 8 R. Di Corato, G. Bealle, J. Kolosnjaj-Tabi, A. Espinosa, O. Clement, A. K. Silva, C. Menager and C. Wilhelm, *ACS nano*, 2015, **9**, 2904-2916.
- 9 C. S. Shemesh, D. Moshkelani and H. Zhang, *Pharm. Res.*, 2015, **32**, 1604-1614.
- 10 A. Yuan, X. Tang, X. Qiu, K. Jiang, J. Wu and Y. Hu, *Chem. Commun.*, 2015, **51**, 3340-3342.
- 11 J. Kim, O. A. Santos and J. H. Park, *J. Control. Release*, 2014, **191**, 98-104.
- 12 G. Saravanakumar, J. Lee, J. Kim and W. J. Kim, *Chem. Commun.*, 2015, **51**, 9995-9998.
- 13 D. Ling, B. C. Bae, W. Park and K. Na, *Biomaterials*, 2012, **33**, 5478-5486.
- 14 A. Kano, Y. Taniwaki, I. Nakamura, N. Shimada, K. Moriyama and A. Maruyama, *J. Control. Release*, 2013, **167**, 315-321.
- 15 J. Tu, T. Wang, W. Shi, G. Wu, X. Tian, Y. Wang, D. Ge and L. Ren, *Biomaterials*, 2012, **33**, 7903-7914.
- 16 H. Benachour, A. Seve, T. Bastogne, C. Frochot, R. Vanderesse, J. Jasniewski, I.

- Miladi, C. Billotey, O. Tillement, F. Lux and M. Barberi-Heyob, *Theranostics*, 2012, **2**, 889-904.
- 17 E. Secret, M. Maynadier, A. Gallud, A. Chaix, E. Bouffard, M. Gary-Bobo, N. Marcotte, O. Mongin, K. El Cheikh, V. Hugues, M. Auffan, C. Frochot, A. Morere, P. Maillard, M. Blanchard-Desce, M. J. Sailor, M. Garcia, J. O. Durand and F. Cunin, *Adv. Mater.*, 2014, **26**, 7643-7648.
- 18 Y. I. Park, H. M. Kim, J. H. Kim, K. C. Moon, B. Yoo, K. T. Lee, N. Lee, Y. Choi, W. Park, D. Ling, K. Na, W. K. Moon, S. H. Choi, H. S. Park, S. Y. Yoon, Y. D. Suh, S. H. Lee and T. Hyeon, *Adv. Mater.*, 2012, **24**, 5755-5761.
- 19 J. Shan, S. J. Budijono, G. Hu, N. Yao, Y. Kang, Y. Ju and R. K. Prud'homme, *Adv. Funct. Mater.*, 2011, **21**, 2488-2495.
- 20 C. Wang, L. Cheng, Y. Liu, X. Wang, X. Ma, Z. Deng, Y. Li and Z. Liu, *Adv. Funct. Mater.*, 2013, **23**, 3077-3086.
- 21 J. K. Rhee, M. Baksh, C. Nycholat, J. C. Paulson, H. Kitagishi and M. G. Finn, *Biomacromolecules*, 2012, **13**, 2333-2338.
- 22 H. Kim, Y. Kim, I. H. Kim, K. Kim and Y. Choi, *Theranostics*, 2013, **4**, 1-11.
- 23 W. J. Syu, H. P. Yu, C. Y. Hsu, Y. C. Rajan, Y. H. Hsu, Y. C. Chang, W. Y. Hsieh, C. H. Wang and P. S. Lai, *Small*, 2012, **8**, 2060-2069.
- 24 J. Chen, T. W. Liu, P. C. Lo, B. C. Wilson and G. Zheng, *Bioconjugate Chem.*, 2009, **20**, 1836-1842.
- 25 T. M. Mawn, A. V. Popov, N. J. Beardsley, K. Stefflova, M. Milkevitch, G. Zheng and E. J. Delikatny, *Bioconjugate Chem.*, 2011, **22**, 2434-2443.

- 26 E. Clo, J. W. Snyder, N. V. Voigt, P. R. Ogilby and K. V. Gothelf, *J. Am. Chem. Soc.*, 2006, **128**, 4200-4201.
- 27 I. V. Nesterova, S. S. Erdem, S. Pakhomov, R. P. Hammer and S. A. Soper, *J. Am. Chem. Soc.*, 2009, **131**, 2432-2433.
- 28 W. Fan, W. Bu, B. Shen, Q. He, Z. Cui, Y. Liu, X. Zheng, K. Zhao and J. Shi, *Adv. Mater.*, 2015, **27**, 4155-4161.
- 29 C. S. Jin, L. Cui, F. Wang, J. Chen and G. Zheng, *Adv. Healthc. Mat.*, 2014, **3**, 1240-1249.
- 30 L. Huang, J. Zhao, S. Guo, C. Zhang and J. Ma, *J. Org. Chem.*, 2013, **78**, 5627-5637.
- 31 P. Yang, J. Zhao, W. Wu, X. Yu and Y. Liu, *J. Org. Chem.*, 2012, **77**, 6166-6178.
- 32 Y. Chen, J. Zhao, H. Guo and L. Xie, *The J. Org. Chem.*, 2012, **77**, 2192-2206.
- 33 W. Wu, H. Guo, W. Wu, S. Ji and J. Zhao, *J. Org. Chem.*, 2011, **76**, 7056-7064.
- 34 L. Huang, X. Yu, W. Wu and J. Zhao, *Org. Lett.*, 2012, **14**, 2594-2597.
- 35 H. He, P. C. Lo, S. L. Yeung, W. P. Fong and D. K. Ng, *J. Med. Chem.*, 2011, **54**, 3097-3102.
- 36 M. R. Ke, S. L. Yeung, D. K. Ng, W. P. Fong and P. C. Lo, *J. Med. Chem.*, 2013, **56**, 8475-8483.
- 37 S. Erbas-Cakmak and E. U. Akkaya, *Org. Lett.*, 2014, **16**, 2946-2949.
- 38 H. J. Cho, H. Y. Yoon, H. Koo, S. H. Ko, J. S. Shim, J. H. Lee, K. Kim, I. C. Kwon and D. D. Kim, *Biomaterials*, 2011, **32**, 7181-7190.
- 39 K. Y. Choi, K. H. Min, H. Y. Yoon, K. Kim, J. H. Park, I. C. Kwon, K. Choi and

- S. Y. Jeong, *Biomaterials*, 2011, **32**, 1880-1889.
- 40 H. J. Cho, I. S. Yoon, H. Y. Yoon, H. Koo, Y. J. Jin, S. H. Ko, J. S. Shim, K. Kim, I. C. Kwon and D. D. Kim, *Biomaterials*, 2012, **33**, 1190-1200.
- 41 D. S. Kwag, K. Park, K. T. Oh and E. S. Lee, *Chem. Commun.*, 2013, **49**, 282-284.
- 42 L. Qiu, Z. Li, M. Qiao, M. Long, M. Wang, X. Zhang, C. Tian and D. Chen, *Acta Biomater.*, 2014, **10**, 2024-2035.
- 43 W. Miao, G. Shim, C. M. Kang, S. Lee, Y. S. Choe, H. G. Choi and Y. K. Oh, *Biomaterials*, 2013, **34**, 9638-9647.
- 44 N. Kotagiri, G. P. Sudlow, W. J. Akers and S. Achilefu, *Nat. Nanotech.*, 2015, **10**, 370-379.
- 45 M. A. Sowers, J. R. McCombs, Y. Wang, J. T. Paletta, S. W. Morton, E. C. Dreaden, M. D. Boska, M. F. Ottaviani, P. T. Hammond, A. Rajca and J. A. Johnson, *Nat. Commun.*, 2014, **5**, 5460.
- 46 J. Yu, C. H. Hsu, C. C. Huang and P. Y. Chang, *ACS. Appl. Mater. Inter.*, 2015, **7**, 432-441.
- 47 J. T. Lau, P. C. Lo, X. J. Jiang, Q. Wang and D. K. Ng, *J. Med. Chem.*, 2014, **57**, 4088-4097.
- 48 J. Fang, H. Nakamura and H. Maeda, *Adv. Drug. Deliver. Rev.*, 2011, **63**, 136-151.
- 49 H. Kobayashi, R. Watanabe and P. L. Choyke, *Theranostics*, 2013, **4**, 81-89.
- 50 J. W. Nichols and Y. H. Bae, *J. Control. Release*, 2014, **190**, 451-464.

Graphical Abstract



Specific targeting and on-site activated diiodostyryl bodipy conjugated hyaluronic acid nanoparticles (DBHA-NPs) have been synthesized through self-assembly, which not only can effectively suppress tumor growth, but also diagnose the tumor exactly and reduce side effect for patients significantly.